Published by Nigerian Society of Physical Sciences. Hosted by FLAYOO Publishing House LTD

Recent Advances in Natural Sciences

Journal Homepage: https://flayoophl.com/journals/index.php/rans

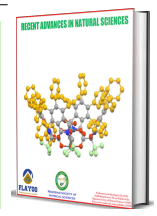

Preparation of baobab shell activated carbon/hematite composite for enhanced adsorption of Congo red dye from aqueous medium

Zuliat O. Opadiran[a,b], Mojeed O. Bello[a,*], Nasiru Abdus-Salam[a,**]

[a]*Department of Chemistry, University of Ilorin, P.M.B. 1515, Ilorin, Nigeria*
[b]*Department of Chemistry and Industrial Chemistry, Kwara State University, Malete, P.M.B. 1530, Ilorin, Nigeria*

ARTICLE INFO

Article history:
Received: 15 April 2026
Received in revised form: 27 July 2026
Accepted: 23 August 2026
Available online: 22 September 2026

Keywords: Adsorption, Activated carbon, Baobab, Congo red, Composite

DOI:10.61298/rans.2026.4.2.356

ABSTRACT

Baobab shell activated carbon (BAC), hematite (HEM), and a hematite–baobab shell activated carbon composite (HB) were prepared for the adsorption of Congo red (CR) from an aqueous medium. Physicochemical and spectroscopic investigations were performed on the individual adsorbents and the composite. The effects of concentration, dosage, pH, and contact time on the adsorptive removal process were evaluated. The equilibrium data for BAC and HB fitted the Langmuir isotherm model well, with R^2 values of 0.9954 and 0.9292, respectively. HEM was best described by the Freundlich model ($R^2 = 0.9243$), but also showed a good fit to the Langmuir model ($R^2 = 0.8747$). The Langmuir monolayer adsorption capacities of BAC, HEM, and HB, which are close to the experimental values, were 322.58, 158.73, and 172.41 mg/g, respectively. The pseudo-second-order model best described the adsorption kinetics, suggesting a chemisorption process. BAC, HEM, and HB can be effectively employed in the remediation of wastewater containing anionic dyes such as Congo red. Furthermore, the adsorption capacity of hematite can be enhanced by adding baobab shell activated carbon because of the high adsorption efficiency of BAC alone towards the dye.

1. INTRODUCTION

Dyes are chemical compounds, mostly synthetic, with a particular colour that can be chemically attached to a substrate to impart colour [1]. The textile, paper, leather, plastic, cosmetic, and pharmaceutical industries use dyes [2, 3]. Among these industries, the textile industry uses substantial quantities of water; typically, 1.0 kg of cotton requires 150 L [4]. According to Bharathi and Ramesh [3], the industry ranks first in the use of dyes to colour fibres, and wastewater from textile dyeing contributes significantly to water pollution. This is a serious concern because the wastewater contains highly stable carcinogenic compounds, such as azo dyes.

Azo dyes are the most commonly used dyes, accounting for about 60% of all dyes [5]. Congo red (CR) (disodium 4-amino-3-[4-[4-(1-amino-4-sulfonato-naphthalen-2-yl)diazenylphenyl]phenyl]diazenyl-naphthalene-1-sulfonate) (Figure 1) is a benzidine-based anionic diazo dye with a stable structure that makes it difficult to biodegrade and gives it a strong affinity for cellulose fibres [6, 7]. In addition, the release of untreated Congo red dye effluent into water bodies can

*Corresponding Author Tel. No.: +234-806-715-1253.
**Corresponding Author Tel. No.: +234-803-395-0752.
e-mail: bello.mo@unilorin.edu.ng (Mojeed O. Bello), nasal@unilorin.edu.ng (Nasiru Abdus-Salam)

impair photosynthesis by reducing sunlight penetration and, in extreme situations, can cause aquatic life to suffocate because of a substantial reduction in oxygen levels [8, 9]. It also acts as a skin and eye irritant in humans, and its decomposition results in carcinogenic products [10].

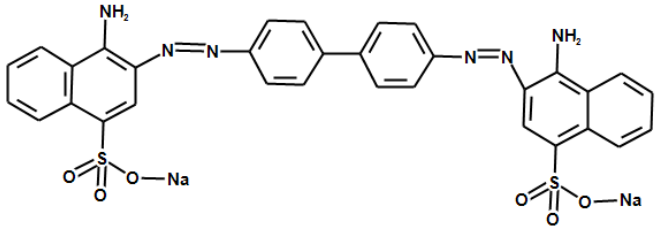

Figure 1. Molecular structure of Congo red dye.

Several methods have been employed to treat Congo red dye, including photocatalytic degradation [11], advanced oxidation processes [12], ultrafiltration, flocculation/electrocoagulation, and biological processes using fungi, bacteria, and plants [6, 13]. Nevertheless, these techniques often entail high costs, limited removal efficiency, and the risk of generating secondary pollutants. In contrast, adsorption has attracted significant interest because of its high adsorption capacity, simple operation, cost-effectiveness, eco-friendliness, and the wide range of available adsorbent materials [14].

Iron oxides are mineral compounds widely distributed in nature and occur in different polymorphic forms [15]. Because of their low toxicity, chemical inertness, biocompatibility, and the possibility of synthesising them in the laboratory from various iron precursors at relatively low cost, iron oxides have garnered significant attention [2]. They occur in three commonly cited forms: hematite (α-Fe_2O_3), maghemite (γ-Fe_2O_3), and magnetite (Fe_3O_4) [16]. Iron oxide materials have been used in water-treatment technology for several years [17].

Hematite is the most stable among the iron oxides under ambient conditions [18]. It is a cost-effective, non-hazardous, and versatile material. Hematite is widely used as a catalyst in industrial synthesis, as a pigment, and in batteries [19, 20]. Compared with other oxide forms of iron, hematite is easier to synthesise [15, 21]. It can be prepared by different techniques, such as precipitation, sol–gel [22, 23], hydrolysis, and hydrothermal methods [24].

Various adsorbents have been studied for their ability to remove dyes from aqueous solutions, including goethite [25], burned roots of *Eichhornia crassipes* [6], a chitosan/hematite nanocomposite [2], and ackee apple pods [26]. This study assesses the efficacy of synthetic hematite, baobab shell activated carbon, and a hematite–baobab shell activated carbon composite for the adsorptive removal of Congo red dye. It also examines how various adsorption parameters influence adsorption capacity in batch mode.

2. MATERIALS AND METHODS

2.1. MATERIALS

The baobab fruit shell used in this work for the production of activated carbon was obtained from a baobab tree at the University of Ilorin. All reagents were of analytical grade and were obtained from Sigma-Aldrich. The chemicals included ferric nitrate [$Fe(NO_3)_3{\cdot}9H_2O$], orthophosphoric acid (85% H_3PO_4), sodium hydrogen carbonate ($NaHCO_3$), potassium hydroxide (KOH), potassium chloride (KCl), sodium hydroxide (NaOH), hydrochloric acid (HCl), and Congo red ($C_{32}H_{22}N_6Na_2O_6S_2$).

2.2. PREPARATION OF BAOBAB SHELL ACTIVATED CARBON

The baobab fruit shell was broken into smaller pieces, thoroughly washed with deionised water to eliminate impurities, and air-dried for 48 h. The baobab shell fragments were impregnated with 85% orthophosphoric acid (H_3PO_4) at a weight ratio of 1:1.75 (w/w) for 24 h, then washed to neutral pH and dried at room temperature. The dried baobab was carbonised for 3 h in a furnace at 500 °C. The as-prepared carbon was washed to eliminate residual acid, dried in an oven at 105 °C for 30 min, pulverised, and then sieved using a 90 μm mesh. The resulting material, referred to as BAC, was stored in an airtight container for further use.

2.3. SYNTHESIS OF HEMATITE

Hematite was synthesised in the laboratory using a modified ferrihydrite method [31]. For the synthesis, 300 mL of 1.0 M KOH was added to 500 mL of 0.1 M $Fe(NO_3)_3{\cdot}9H_2O$. Then, 50 mL of 1.0 M $NaHCO_3$ was added to the resulting brown precipitate. The suspension (pH 8–9) was maintained in a closed polypropylene beaker at 90 °C for 48 h. Each solution was preheated to 90 °C before being combined to form the mixture. The final product, hematite (HEM), was centrifuged, filtered, and dialysed in deionised water to remove nitrates and was then dried in an oven at 40 °C.

2.4. PREPARATION OF HEMATITE–BAOBAB SHELL ACTIVATED CARBON COMPOSITE

The composite was prepared by adding 27 g of baobab shell activated carbon (BAC) to 500 mL of a 0.1 M $Fe(NO_3)_3{\cdot}9H_2O$ solution with continuous stirring. The mixture was then treated with 300 mL of 1.0 M KOH to facilitate precipitation, followed by the addition of 50 mL of 1.0 M $NaHCO_3$. The resulting suspension was maintained in a closed polypropylene beaker at 90 °C for 48 h. The hematite–baobab activated carbon composite was then filtered and washed repeatedly with deionised water until the filtrate reached a pH of 8–9. The obtained precipitate was crushed, oven-dried at 90 °C, and stored in an airtight container.

2.5. CHARACTERISATION

Functional groups on the adsorbents were identified using Fourier-transform infrared spectroscopy (FTIR; Thermo Scientific Nicolet IS5). Surface morphology was observed by scanning electron microscopy (SEM; ASPEX 3020). The X-ray diffraction (XRD) peaks of the synthesised hematite were also obtained.

The point of zero charge (pH_{PZC}) of the adsorbents was determined using the pH-drift method with 0.1 M KCl solution. The initial pH values (pH_0) of the KCl solution, ranging from 2.0 to 12.0, were adjusted using either 0.1 M HCl or 0.1 M NaOH. Subsequently, 0.02 g of each adsorbent was added separately to

50 mL conical flasks containing the salt solutions at the respective pH values. The flasks were sealed and agitated in an orbital shaker for 24 h, after which the final pH (pH_f) was measured. The pH_{PZC} value was obtained from the plot of ($pH_f - pH_0$) versus pH_0 at the point where the curve intersects the zero line [26].

2.6. ADSORPTION EXPERIMENTS

Batch adsorption experiments were conducted to evaluate the effects of initial Congo red (CR) concentration, adsorbent dosage, pH, and contact time on the adsorption performance of BAC, HEM, and HB. In a typical experiment, 0.05 g of adsorbent was added to 25 mL of CR solution at initial concentrations ranging from 100 to 1000 mg/L in a 100 mL conical flask. The mixtures were agitated on an orbital shaker at 25 °C for 3 h to attain equilibrium. Subsequently, 10 mL of the suspension was withdrawn and centrifuged at 2500 rpm for 10 min. The residual CR concentration in the supernatant was determined using a UV–visible spectrophotometer at a maximum wavelength (λ_{max}) of 495 nm. The influence of adsorbent dosage (0.012–0.062 g), pH (1–10), and contact time (10–180 min) was systematically investigated. Equations (1) and (2) were used to determine the amount (q_e) and percentage of CR adsorbed by the adsorbents, respectively.

$$q_e = \frac{C_0 - C_f}{M} \times V, \tag{1}$$

$$\% \text{ adsorption} = \frac{C_0 - C_f}{C_0} \times 100, \tag{2}$$

where C_0 and C_f (mg/L) are the initial and final concentrations of CR solution, respectively, V (L) is the volume of solution, M (g) is the mass of adsorbent, and q_e (mg/g) is the quantity of dye adsorbed.

2.7. ADSORPTION ISOTHERM

The adsorption equilibrium data were described using the Langmuir, Freundlich, and Temkin adsorption isotherm models [equations (3a), (4) and (5a), respectively].

$$\frac{C_e}{q_e} = \frac{1}{q_m K_L} + \frac{C_e}{q_m}, \tag{3a}$$

$$R_L = \frac{1}{1 + K_L C_0}, \tag{3b}$$

$$\log q_e = \log K_f + \frac{1}{n} \log C_e, \tag{4}$$

$$q_e = B \ln A + B \ln C_e, \tag{5a}$$

$$B = \frac{RT}{b}. \tag{5b}$$

Here, C_0 and C_e (mg/L) are the initial and equilibrium concentrations of adsorbate, respectively; q_e (mg/g) is the amount of adsorbate adsorbed per unit mass of adsorbent; q_m (mg/g) is the monolayer adsorption capacity; K_L (L/mg) is the Langmuir adsorption constant; R_L is the separation factor; n is an empirical parameter related to adsorption intensity; K_f (mg/g) is the Freundlich constant representing adsorption capacity; A (L/g) is the Temkin isotherm equilibrium binding constant; b (J/mol) is the Temkin isotherm constant related to the heat of adsorption; R (8.314 J/mol K) is the gas constant; and T (K) is the absolute temperature.

2.8. ADSORPTION KINETICS

The experimental data from the contact-time study were fitted to pseudo-first-order and pseudo-second-order equations [equations 6 and (7), respectively].

$$\ln(q_e - q_t) = \ln q_e - k_1 t, \tag{6}$$

$$\frac{t}{q_t} = \frac{1}{k_2 q_e^2} + \frac{1}{q_e} t, \tag{7}$$

where k_1 (min^{-1}) is the rate constant of pseudo-first-order adsorption, k_2 [g/(mg min)] is the rate constant of pseudo-second-order adsorption, and q_e and q_t (mg/g) are the quantities of adsorbate adsorbed at equilibrium and at time t, respectively.

3. RESULTS AND DISCUSSION

3.1. CHARACTERISATION

The physicochemical properties of the three as-prepared adsorbents are presented in Table 1. Activated carbon (BAC) is black, whereas hematite (HEM) is brown. The introduction of activated carbon into hematite during composite formation resulted in a black colour for the composite (HB). The percentage yield of activated carbon relative to the initial biomass at the carbonisation temperature indicates that the biomass contains a significant amount of carbonaceous material. HEM has the highest bulk density, and this decreased in HM with the introduction of BAC. This is an improvement in terms of lower bulk density [32]. The pH of the three adsorbents ranges from 6.84 to 7.45. The points of zero charge (pH_{PZC}) for BAC, HEM, and HB (Figure 2a) are 8, 8.3, and 8.3, respectively. Above these pH_{PZC} values, adsorption of cations is favoured, whereas adsorption of anions is favoured below them [33]. The lower ash content and higher iodine number of the activated carbon indicate good stability and better performance, respectively [34].

Table 1. Physicochemical properties of BAC, HEM, and HB adsorbents.

Physicochemical parameter	BAC	HEM	HB
Appearance	Black	Brown	Black
Yield (%)	50	ND	ND
Bulk density (g/cm^3)	0.406	1.43	0.498
pH	6.84	7.45	7.24
pH_{PZC}	8	8.3	8.3
Moisture content (%)	12	ND	ND
Ash content (%)	7.33	ND	ND
Iodine value	507.6	ND	ND

ND: Not determined.

Figure 2b shows the FTIR spectra of BAC, HEM, and HB. The FTIR spectrum of the synthesised Fe_2O_3 sample shows a broad band at 3404.11 cm^{-1} that can be assigned to the O–H stretching vibration of H_2O molecules. The peak at 1626.43 cm^{-1} can be assigned to the bending vibrations of H_2O molecules. O–H deformation is responsible for the band at 939.69 cm^{-1}, and the

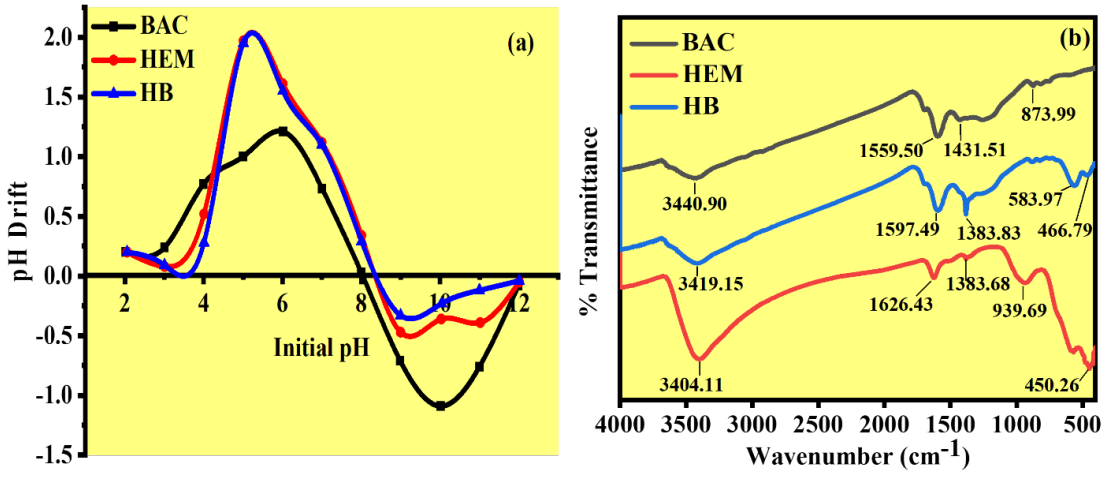

Figure 2. (a) Point of zero charge and (b) FTIR spectra of BAC, HEM, and HB.

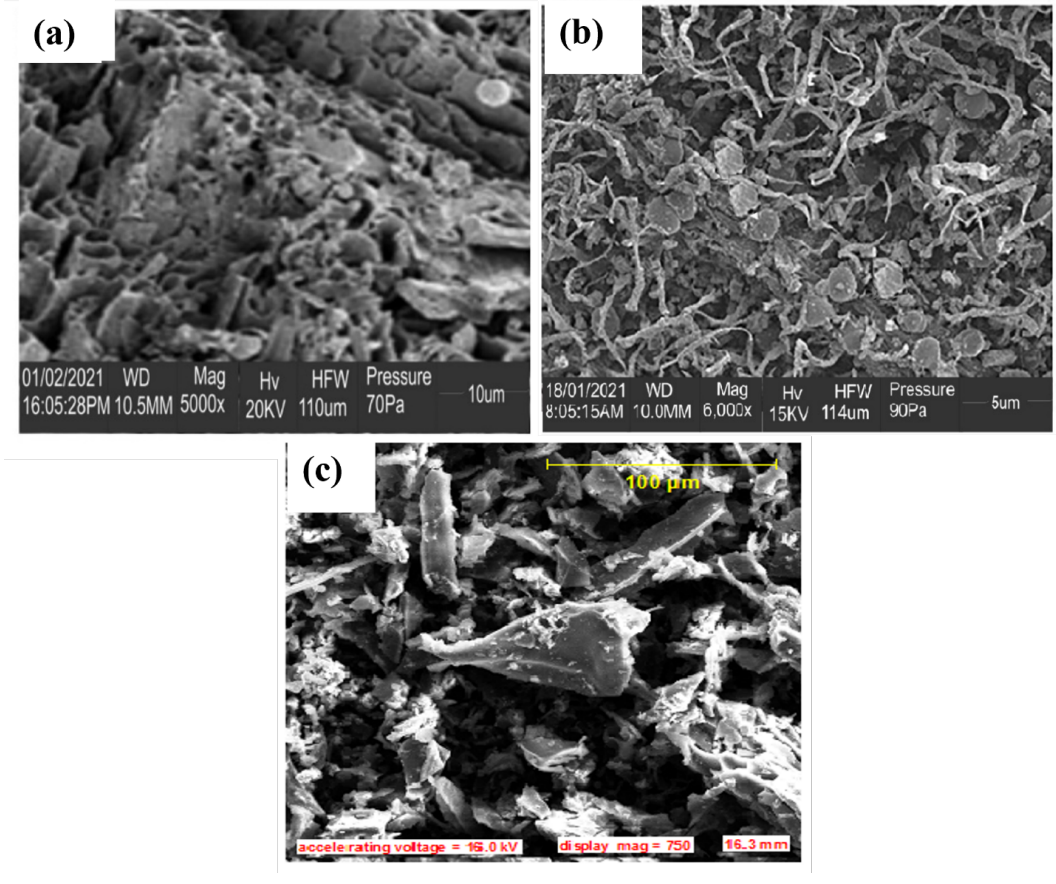

Figure 3. SEM images of (a) BAC, (b) HEM, and (c) HB.

peak at 450.26 cm^{-1} indicates the presence of the Fe–O vibration mode of Fe_2O_3 [22, 35].

In BAC, the band observed at 3440.90 cm^{-1} can be attributed to –OH groups. The peak at 1595.50 cm^{-1} can be attributed to aromatic C=C [36] or C–O–C (ester, ether, and phenol) [37]. The weak peak at 873.99 cm^{-1} can be assigned to phosphorus species in the sample. The composite (HB) displays bands observed in the BAC and HEM spectra, with different intensities.

The surface morphologies of BAC, HEM, and HB were analysed from the SEM images. Figure 3b depicts SEM micrograph of HEM, which consists of spherical particles that appear to agglomerate. It also shows irregular thread-like shapes with many pores that may aid adsorption. Figure 3a shows the SEM micrograph of BAC with pores and a honeycomb-like arrangement. The SEM result for HB (Figure 3c) shows irregular, rod-like hematite grains. The external surface of the rod-like structure reveals a crack, suggesting the presence of BAC.

The XRD pattern of hematite (HEM), compared with the ref-

erence obtained from the Materials Project database (card no. mp-19770), is presented in Figure 4. It shows peaks at $2\theta = 23.756°, 32.821°, 35.407°, 40.550°, 49.177°, 53.647°, 62.109°$, and $63.793°$, typical of Fe_2O_3 [38]. Similar XRD diffractograms were previously reported by Adegoke and Adekola [31] and Ibrahim *et al.* [16]. BAC did not exhibit a significant diffraction pattern (Figure not shown) because carbon is amorphous. Consequently, no new peaks were expected for HB apart from those of HEM.

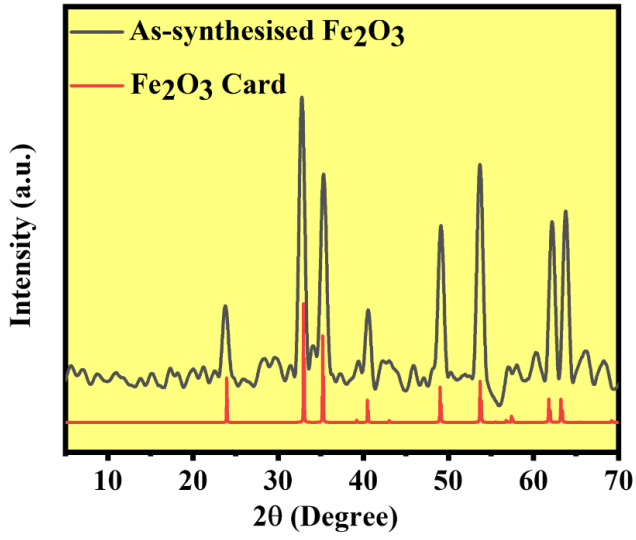

Figure 4. XRD pattern of HEM.

3.2. ADSORPTION EXPERIMENTS

3.2.1. Effect of initial concentration

The adsorption of Congo red on BAC, HEM, and HB was investigated over concentration ranges of 100–1000 mg/L for HEM and HB and 300–1000 mg/L for BAC, as illustrated in Figure 5a. Other parameters, such as adsorbent dosage (0.05 g), pH (6.8), and contact time (180 min), were fixed. The initial dye concentration provides the driving force needed to overcome resistance to mass transfer of dye molecules between the aqueous and solid phases [30]. The amount of Congo red adsorbed increased with increasing initial dye concentration up to 900 mg/L, as shown in Figure 5a, with maximum adsorption capacities of 306.61, 153, and 184.36 mg/g for BAC, HEM, and HB, respectively. The percentage removal decreased with increasing dye concentration because of reduced available surface area and saturation of active sites [39]. Similar trends were reported by Roy and Mondal [6] and Radoor *et al.* [40].

3.2.2. Effect of adsorbent dosage

Figure 5b illustrates how the dosages of BAC, HEM, and HB affect the adsorption of Congo red from aqueous solution at a constant concentration (900 mg/L), pH (6.8), and contact time (180 min). The adsorption capacities decreased as the adsorbent dosage increased. The decrease in adsorption per unit mass with increasing adsorbent dosage may be due to overlapping adsorption sites [41], thereby reducing the concentration of adsorbate molecules per available active site.

3.2.3. Effect of pH

Solution pH is crucial to the dye adsorption process because it influences the active sites on the adsorbent surface and the properties of the dye [13]. A pH range of 1–10, with a fixed dosage (0.012 g), concentration (900 mg/L), and contact time (180 min), was examined to assess the effect of pH. Congo red undergoes a red-to-dark-blue transition in acidic media before turning solid red at pH 6–7 because of protonation or deprotonation. Figure 5c shows that the adsorption capacity decreased as pH increased from 1 to 10. The removal percentages for BAC, HEM, and HB were 98.3%, 99.89%, and 99.5%, respectively, at pH 2, where the maximum CR adsorption was observed. All adsorbents have a pH_{PZC} between 8 and 8.3. The surface of an adsorbent is negatively charged at $pH > pH_{PZC}$, which inhibits the adsorption of anionic dye species because of electrostatic repulsion between the negatively charged surface and dye molecules. The higher adsorption of CR at low pH is due to strong electrostatic attraction between anionic CR molecules and the cationic adsorbent surface [25, 26].

3.2.4. Effect of contact time

The influence of contact time on CR adsorption at a constant concentration of 900 mg/L, pH 2, and adsorbent dosage of 0.012 g is depicted in Figure 5d. Adsorption was rapid during the initial contact period (0–45 min for BAC and 0–10 min for both HEM and HB) because of the availability of active sites. Then the adsorption rate gradually decreased, reaching equilibrium within 45 and 180 min for BAC; 10 and 180 min for HEM; and 10 and 120 min for HB. At this stage, fewer binding sites are available. Similar behaviour was reported by Wanyonyi *et al.* [9] and Roy and Mondal [6]. At equilibrium, 945.37 mg/g (52.52%), 1796.56 mg/g (99.81%), and 1797.62 mg/g (99.88%) were achieved for BAC, HEM and HB, respectively.

3.3. ADSORPTION ISOTHERM

Adsorption isotherms describe equilibrium relationships between adsorbents and adsorbates at a constant temperature. In this study, data from the initial-concentration experiments were analysed using the Langmuir, Freundlich, and Temkin isotherm models. Table 2 lists the parameters of the isotherm models, while the respective plots are shown in Figure 6a–c. Based on the regression coefficients (R^2) shown in Table 2, the order of fit is Langmuir (0.9954) > Temkin (0.9468) > Freundlich (0.9165) for BAC; Freundlich (0.9243) > Langmuir (0.8747) > Temkin (0.803) for HEM; and Langmuir (0.9292) > Freundlich (0.8771) > Temkin (0.8614) for HB.

The fit of the equilibrium data for BAC and HB (excellent) and HEM (good) to the Langmuir model assumes that adsorbate adsorption occurs as a monolayer on homogeneous adsorbent surfaces with energetically identical sites available for interaction with the adsorbate [42]. Further analysis of the Langmuir model using the separation factor (R_L) showed that the values for CR are in the range $0 < R_L < 1$, indicating favourable adsorption of CR by the adsorbents. Cong *et al.* [43] and Su *et al.* [44] reported similar observations for Congo red adsorption. However,

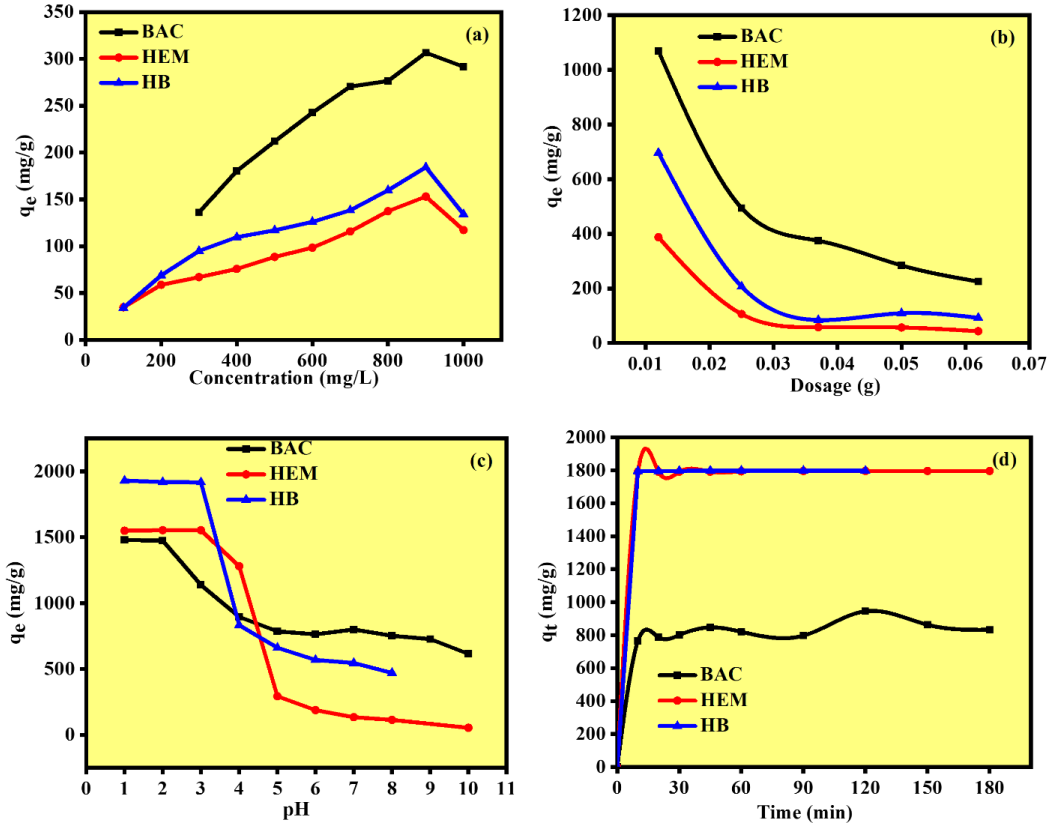

Figure 5. Effect of (a) concentration, (b) adsorbent dosage, (c) pH, and (d) contact time on the adsorption of Congo red dye onto BAC, HEM, and HB.

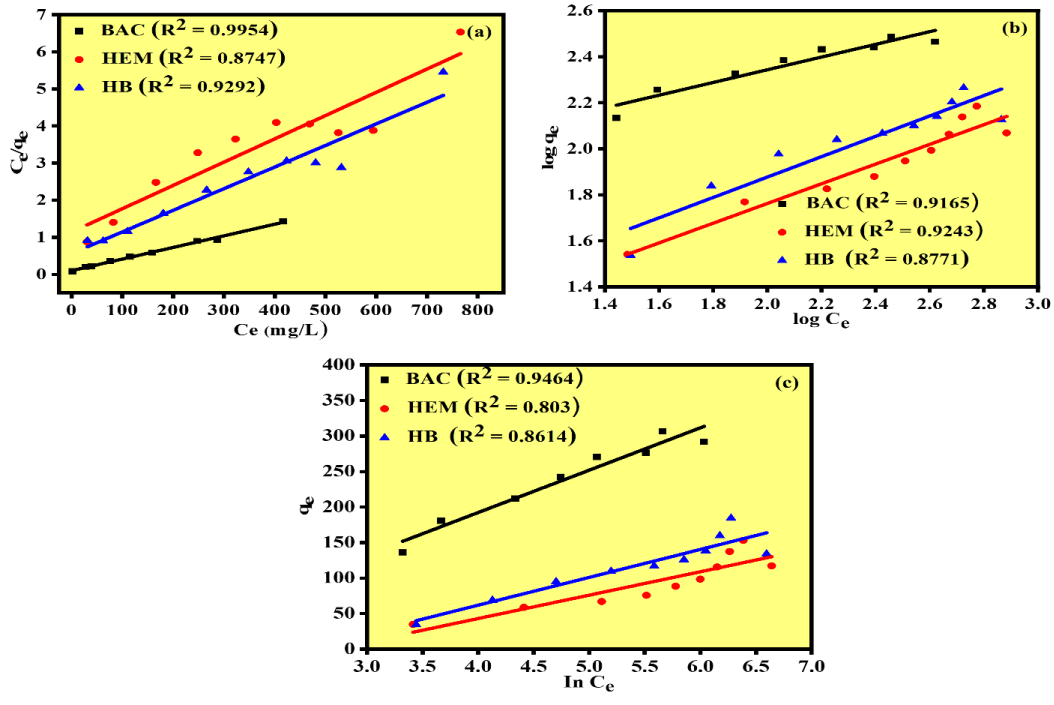

Figure 6. (a) Langmuir isotherm, (b) Freundlich isotherm, and (c) Temkin isotherm for the adsorption of Congo red dye onto BAC, HEM, and HB.

the high R^2 values from the Freundlich model indicate some heterogeneity of the surfaces. Table 3 compares the monolayer adsorption capacity (q_m) values obtained in this study with those reported for other adsorbents used for Congo red removal.

The higher Freundlich R^2 value for HEM than for BAC and HB suggests that the adsorption mechanism involved a more het-

Table 2. Isotherm parameters for the adsorption of Congo red dye onto BAC, HEM, and HB.

Adsorption isotherm	Parameter	BAC	HEM	HB
Langmuir	q_m (mg/g)	322.58	158.73	172.41
	K_L (L/mg)	0.029	5.519×10^{-3}	0.0103
	R_L	0.037	0.168	0.097
	R^2	0.9954	0.8747	0.9292
Freundlich	n	3.621	2.335	2.259
	$1/n$	0.276	0.428	0.443
	K_f (L/mg)	61.787	8.048	9.811
	R^2	0.9165	0.9243	0.8771
Temkin	B	59.673	32.956	39.254
	b (J/mol)	41.519	75.178	63.116
	A (L/g)	0.459	0.068	0.088
	R^2	0.9468	0.803	0.8614

Table 3. Comparison of the monolayer adsorption capacity of BAC, HEM, and HB with other adsorbents for Congo red dye.

Adsorbent	q_m (mg/g)	Reference
BAC	322.58	This study
HEM	158.73	This study
HB	172.41	This study
Groundnut shells charcoal (GNC)	117.6	[27]
Eichhornia charcoal (EC)	56.8	[27]
Cabbage waste powder	2.313	[28]
α-Fe_2O_3 nanorod	78.13	[29]
γ-Fe_2O_3 nanorod	232.56	[29]
Activated carbon coffee waste (ACCW)	90.90	[30]
Burned root of *Eichhornia crassipes* (BREC)	14.49	[6]

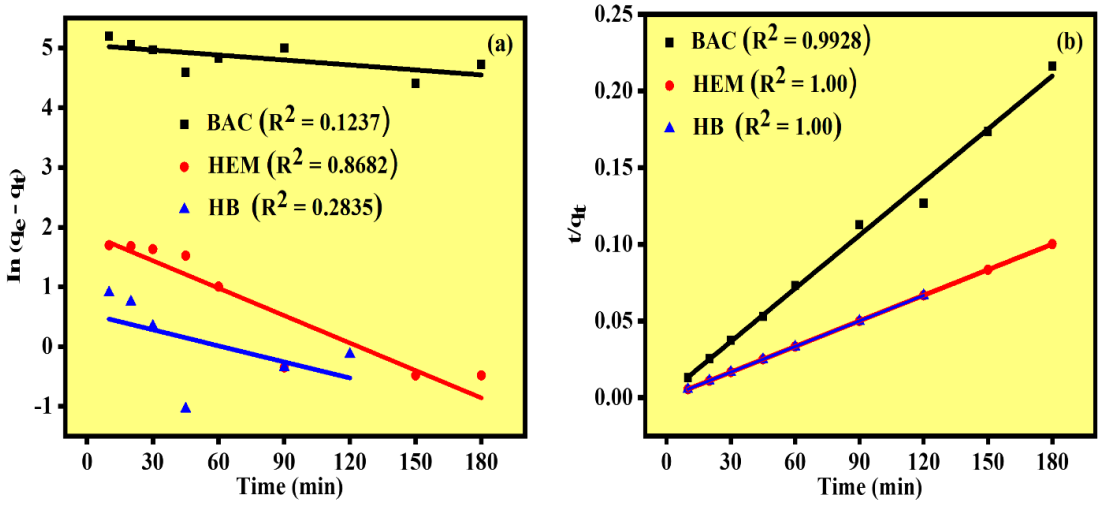

Figure 7. (a) Pseudo-first-order and (b) pseudo-second-order kinetics for the adsorption of Congo red dye onto BAC, HEM, and HB.

erogeneous surface. Analysis of n and $1/n$ provides information about adsorption intensity and surface heterogeneity. Values of $1/n$ within the range 0–1 indicate favourable Freundlich adsorption. From Table 2, values of $n > 1$ indicate a high affinity of the dye for the three adsorbents, consistent with chemisorption. Similar findings were reported by Kaur *et al.* [27] and Omidi Khaniabadi *et al.* [7].

The Temkin model states that the heat of adsorption of every molecule in the layer decreases linearly with coverage because of interactions between adsorbents and adsorbates [45]. For BAC, HEM, and HB, the Temkin constant b, which is related to the heat of adsorption, is 41.519, 75.178, and 63.116 J/mol, respectively. The lower BAC value indicates improved interaction between BAC and the dye.

3.4. ADSORPTION KINETICS

The adsorption data obtained as a function of contact time were analysed using the two most common kinetic models, pseudo-

Table 4. Kinetic parameters for the adsorption of Congo red dye onto BAC, HEM, and HB.

Adsorbent	$q_{e,\exp}$ (mg/g)	Pseudo-first-order			Pseudo-second-order		
		k_1 (min^{-1})	$q_{e,\text{cal}}$ (mg/g)	R^2	k_2 [g/(mg min)]	$q_{e,\text{cal}}$ (mg/g)	R^2
BAC	945	0.0095	156.66	0.1237	7.579×10^{-4}	833.33	0.9928
HEM	1796.56	0.015	6.675	0.8682	9×10^{-3}	1666.67	1
HB	1797.62	0.009	1.732	0.2835	0.12	1666.67	1

first-order and pseudo-second-order, as depicted in Figure 7a and b, respectively. The best-fit model was selected based on the proximity of the correlation coefficient (R^2) to unity and the agreement between the experimental quantity adsorbed ($q_{e,\exp}$) and the calculated quantity ($q_{e,\text{cal}}$). As shown in Table 4, the pseudo-second-order kinetic model exhibited excellent linearity, with R^2 values close to unity. The pseudo-first-order model yielded an R^2 value of 0.8682 for HEM. The pseudo-first-order model does not describe the kinetic data for dye adsorption onto the adsorbents because of the significant discrepancy between the calculated and experimental values of q_e. The pseudo-second-order model best describes Congo red adsorption onto the three adsorbents, with $q_{e,\text{cal}}$ and $q_{e,\exp}$ in relatively close agreement. This suggests that chemisorption may be involved in the adsorption process through a mechanism involving the exchange or sharing of valence electrons between the adsorbate and adsorbent. Similar results were observed for Congo red adsorption from aqueous solution onto tea waste [46] and for Congo red removal by biowaste materials [27].

4. CONCLUSION

The adsorption efficiencies of baobab shell activated carbon (BAC), hematite (HEM), and the hematite–baobab shell activated carbon composite (HB) towards Congo red (CR) dye were studied. The adsorption process was influenced by the adsorption parameters, especially pH and concentration. Maximum adsorption was observed at pH 2 and an optimum concentration of 900 mg/L. The Langmuir model described the adsorption data for CR onto BAC and HB, whereas the Freundlich model best fitted HEM. The adsorption process fitted pseudo-second-order kinetics well. Based on the results of this study, BAC, HEM, and HB can be effectively employed to treat dye-laden wastewater. The adsorption capacity of HEM for Congo red dye was improved by incorporating BAC, although BAC alone showed the highest adsorption based on the experimental concentration and dosage results and the Langmuir monolayer capacities. Consequently, biomass can provide sustainable materials for water remediation.

DATA AVAILABILITY

The authors declare that the data supporting the findings of this study are available within the paper. Raw data files in another format are available from the corresponding author upon reasonable request.

DECLARATION OF COMPETING INTEREST

The authors declare that they have no known competing financial interests or personal relationships that could have appeared to influence the work reported in this manuscript.

FUNDING

This research received no specific grant.

ACKNOWLEDGMENT

The authors sincerely appreciate the support of the academic and technical staff of the Department of Chemistry, University of Ilorin, Nigeria.

References

[1] Z. Li, H. Hanafy, L. Zhang, L. Sellaoui, M. Schadeck Netto, M. L. S. Oliveira, M. K. Seliem, G. L. Dotto, A. Bonilla-Petriciolet & Q. Li, "Adsorption of Congo red and methylene blue dyes on an ashitaba waste and a walnut shell-based activated carbon from aqueous solutions: Experiments, characterization and physical interpretations", Chemical Engineering Journal **388** (2020) 124263. https://doi.org/10.1016/j.cej.2020.124263.

[2] G. Ohemeng-Boahen, D. D. Sewu, H. N. Tran & S. H. Woo, "Enhanced adsorption of Congo red from aqueous solution using chitosan/hematite nanocomposite hydrogel capsule fabricated via anionic surfactant gelation", Colloids and Surfaces A: Physicochemical and Engineering Aspects **625** (2021) 126911. https://doi.org/10.1016/j.colsurfa.2021.126911.

[3] K. S. Bharathi & S. T. Ramesh, "Removal of dyes using agricultural waste as low-cost adsorbents: A review", Applied Water Science **3** (2013) 773. https://doi.org/10.1007/s13201-013-0117-y.

[4] S. Afroze & T. K. Sen, "A review on heavy metal ions and dye adsorption from water by agricultural solid waste adsorbents", Water, Air, & Soil Pollution **229** (2018) 225. https://doi.org/10.1007/s11270-018-3869-z.

[5] S. Benkhaya, S. M'rabet & A. El Harfi, "Classifications, properties, recent synthesis and applications of azo dyes", Heliyon **6** (2020) e03271. https://doi.org/10.1016/j.heliyon.2020.e03271.

[6] T. K. Roy & N. K. Mondal, "Biosorption of Congo red from aqueous solution onto burned root of Eichhornia crassipes biomass", Applied Water Science **7** (2017) 1841. https://doi.org/10.1007/s13201-015-0358-z.

[7] Y. Omidi Khaniabadi, M. J. Mohammadi, M. Shegerd, S. Sadeghi, S. Saeedi & H. Basiri, "Removal of Congo red dye from aqueous solutions by a low-cost adsorbent: Activated carbon prepared from aloe vera leaves shell", Environmental Health Engineering and Management Journal **4** (2017) 29. https://doi.org/10.15171/EHEM.2017.05.

[8] F. Parvin, S. Islam, Z. Urmy & S. Ahmed, "A study on the solutions of environment pollutions and worker's health problems caused by textile manufacturing operations", Biomedical Journal of Scientific & Technical Research **28** (2020) 21831. https://doi.org/10.26717/BJSTR.2020.28.004692.

[9] W. C. Wanyonyi, J. M. Onyari & P. M. Shiundu, "Adsorption of Congo red dye from aqueous solutions using roots of Eichhornia crassipes: Kinetic and equilibrium studies", Energy Procedia **50** (2014) 862. https://doi.org/10.1016/j.egypro.2014.06.105.

[10] N. B. Swan & M. A. A. Zaini, "Adsorption of malachite green and Congo red dyes from water: Recent progress and future outlook", Ecological Chemistry and Engineering **26** (2019) 119. https://doi.org/10.1515/eces-2019-0009.

[11] N. Laouedj, A. Elaziouti & A. Bekka, "Photodegradation study of Congo red in aqueous solution using ZnO/UV-A: Effect of pH and band gap of other semiconductor groups", Journal of Chemical Engineering & Process Technology **2** (2011) 108. https://doi.org/10.4172/2157-7048.1000108.

[12] J. Gaur, K. Vikrant, K. H. Kim, S. Kumar, M. Pal, R. Badru, S. Masand & J. Momoh, "Photocatalytic degradation of Congo red dye using zinc oxide nanoparticles prepared using Carica papaya leaf extract", Material Today Sustainability **22** (2023) 100339. https://doi.org/10.1016/j.mtsust.2023.100339

[13] K. Wu, X. Pan, J. Zhang, X. Zhang, A. S. Zene & Y. Tian, "Biosorption of Congo red from aqueous solutions based on self-immobilized mycelial

pellets: Kinetics, isotherms, and thermodynamic studies'', ACS Omega **5** (2020) 24601. https://doi.org/10.1021/acsomega.0c03114.

[14] N. A. Qasem, R. H. Mohammed & D. U. Lawal, ''Removal of heavy metal ions from wastewater: A comprehensive and critical review'', npj Clean Water **4** (2021) 1. https://doi.org/10.1038/s41545-021-00127-0.

[15] E. A. Campos, D. V. B. S. Pinto, J. I. S. de Oliveira, E. da C. Mattos & R. de C. L. Dutra, ''Synthesis, characterization and applications of iron oxide nanoparticles—a short review'', Journal of Aerospace Technology and Management **7** (2015) 267. https://doi.org/10.5028/jatm.v7i3.471.

[16] S. M. Ibrahim, M. A. Naghmash & S. A. El-Molla, ''Synthesis and application of nano-hematite on the removal of carcinogenic textile Remazol red dye from aqueous solution'', Desalination and Water Treatment **180** (2020) 370. https://doi.org/10.5004/dwt.2020.25063.

[17] V. A. Grover, J. Hu, K. E. Engates & H. J. Shipley, ''Adsorption and desorption of bivalent metals to hematite nanoparticles'', Environmental Toxicology and Chemistry **31** (2012) 86. https://doi.org/10.1002/etc.712.

[18] K. G. Gareev, ''Diversity of iron oxides: Mechanisms of formation, physical properties and applications'', Magnetochemistry **9** (2023) 119. https://doi.org/10.3390/magnetochemistry9050119.

[19] J. B. Lee, H. J. Kim, J. Lužnik, A. Jelen, D. Pajić, M. Wencka, Z. Jagličić, A. Meden & J. Dolinšek, ''Synthesis and magnetic properties of hematite particles in a 'nanomedusa' morphology'', Journal of Nanomaterials **2014** (2014) 902968. https://doi.org/10.1155/2014/902968.

[20] R. Ramesh, S. Sohila, C. Muthamizhchelvan, M. Rajalakshmi, S. Ramya & S. Ponnusamy, ''Synthesis and vibrational properties of hematite (α-Fe_2O_3) nanoparticles'', Journal of Materials Science: Materials in Electronics **22** (2011) 1357. https://doi.org/10.1007/s10854-011-0313-1.

[21] R. M Cornell, & U. Schwertmann, ''The Iron Oxides: structure, properties, reactions, occurrences and uses, VCH, Weinheim'', (2003), p. 345. http://dx.doi.org/10.1002/3527602097

[22] H. I. Adegoke, F. A. Adekola, O. S. Fatoki & B. J. Ximba, ''Adsorption of Cr(VI) on synthetic hematite (α-Fe_2O_3) nanoparticles of different morphologies'', Korean Journal of Chemical Engineering **31** (2014) 142. https://doi.org/10.1007/s11814-013-0204-7.

[23] I. Herrmann-Geppert, P. Bogdanoff, L. Hepperle & S. Fiechter, ''Hematite (α-Fe_2O_3) photoanodes for the photooxidation of water'', ECS Transactions **41** (2012) 201. https://doi.org/10.1149/1.3702427.

[24] R. Khurram, Z. Wang, M. F. Ehsan, S. Peng, M. Shafiq & B. Khan, ''Synthesis and characterization of an α-Fe_2O_3/ZnTe heterostructure for photocatalytic degradation of Congo red, methyl orange and methylene blue'', RSC Advances **10** (2020) 44997. https://doi.org/10.1039/D0RA06866G.

[25] N. Abdus-Salam, F. A. Ugbe & A. V. I. Ugbe, ''Optimization and sorption isotherms analysis of anionic dye eosin yellow decontamination by goethite adsorbent'', Acta Scientifica Malaysia **4** (2020) 75. https://doi.org/10.26480/asm.02.2020.75.81.

[26] M. O. Bello, N. Abdus-Salam, F. A. Adekola & U. Pal, ''Isotherm and kinetic studies of adsorption of methylene blue using activated carbon from ackee apple pods'', Chemical Data Collections **31** (2021) 100607. https://doi.org/10.1016/j.cdc.2020.100607.

[27] S. Kaur, S. Rani & R. K. Mahajan, ''Adsorption kinetics for the removal of hazardous dye Congo red by biowaste materials as adsorbents'', Journal of Chemistry **2013** (2013) 628582. https://doi.org/10.1155/2013/628582.

[28] J. N. Wekoye, W. C. Wanyonyi, P. T. Wangila & M. K. Tonui, ''Kinetic and equilibrium studies of Congo red dye adsorption on cabbage waste powder'', Environmental Chemistry and Ecotoxicology **2** (2020) 24. https://doi.org/10.1016/j.enceco.2020.01.004.

[29] J. P. Dhal, B. G. Mishra & G. Hota, ''Ferrous oxalate, maghemite and hematite nanorods as efficient adsorbents for decontamination of Congo red dye from aqueous system'', International Journal of Environmental Science and Technology **12** (2015) 1845. https://doi.org/10.1007/s13762-014-0535-x.

[30] R. Lafi, I. Montasser & A. Hafiane, ''Adsorption of Congo red dye from aqueous solutions by prepared activated carbon with oxygen-containing functional groups and its regeneration'', Adsorption Science & Technology **37** (2019) 160. https://doi.org/10.1177/0263617418819227.

[31] H. I. Adegoke & F. A. Adekola, ''Equilibrium sorption of hexavalent chromium from aqueous solution using synthetic hematite'', Colloid Journal **74** (2012) 1. https://doi.org/10.1134/S1061933X12040035.

[32] Z. Liu, B. Mi, Z. Jiang, B. Fei, Z. Cai & X. Liu, ''Improved bulk density of bamboo pellets as biomass for energy production'', Renewable Energy **86** (2016) 1. https://doi.org/10.1016/j.renene.2015.08.011.

[33] X. Liang, G. Wei, J. Xiong, F. Tan, H. He, C. Qu, H. Yin, J. Zhu, R. Zhu, Z. Qin & J. Zhang, ''Adsorption isotherm, mechanism, and geometry of Pb(II) on magnetites substituted with transition metals'', Chemical Geology **470** (2017) 132. https://doi.org/10.1016/j.chemgeo.2017.09.003.

[34] S. Mopoung, P. Moonsri, W. Palas & S. Khumpai, ''Characterization and properties of activated carbon prepared from tamarind seeds by KOH activation for Fe(III) adsorption from aqueous solution'', The Scientific World Journal **2015** (2015) 415961. https://doi.org/10.1155/2015/415961.

[35] J. Sharmila Justus, S. Dawn Dharma Roy & A. Moses Ezhil Raj, ''Synthesis and characterization of hematite nanopowders'', Materials Research Express **3** (2016) 105037. https://doi.org/10.1088/2053-1591/3/10/105037.

[36] E. Vunain, D. Kenneth & T. Biswick, ''Synthesis and characterization of low-cost activated carbon prepared from Malawian baobab fruit shells by H_3PO_4 activation for removal of Cu(II) ions: Equilibrium and kinetics studies'', Applied Water Science **7** (2017) 4301. https://doi.org/10.1007/s13201-017-0573-x.

[37] R. Nedjai, N. A. Kabbashi, M. Z. Alam & M. F. R. Al-Khatib, ''Production and characterization of activated carbon from baobab fruit shells by chemical activation using $ZnCl_2$, H_3PO_4 and KOH'', Journal of Physics: Conference Series **2129** (2021) 012009. https://doi.org/10.1088/1742-6596/2129/1/012009.

[38] M. C. Morris, H. F. McMurdie, E. H. Evans, B. Paretzkin, H. S. Parker, N. C. Panagiotopoulos & C. Hubbard, *Standards X-ray Diffraction Powder Patterns, Section 18: Data for 58 Substances*, U.S. Department of Commerce, National Bureau of Standards, Washington, DC, USA, 1981, p. 37. https://doi.org/10.6028/NBS.MONO.25-18.

[39] N. H. Azmi, U. F. M. Ali, F. Muhammad Ridwan, K. M. Isa, N. Z. Zulkurnai & M. K. Aroua, ''Preparation of activated carbon using sea mango (Cerbera odollam) with microwave-assisted technique for the removal of methyl orange from textile wastewater'', Desalination and Water Treatment **57** (2016) 29143. https://doi.org/10.1080/19443994.2016.1168134.

[40] S. Radoor, J. Karayil, J. Parameswaranpillai & S. Siengchin, ''Removal of anionic dye Congo red from aqueous environment using polyvinyl alcohol/sodium alginate/ZSM-5 zeolite membrane'', Scientific Reports **10** (2020) 15452. https://doi.org/10.1038/s41598-020-72398-5.

[41] J. Godwin, J. R. Njimou, N. Abdus-Salam, P. K. Panda, B. C. Tripathy, M. K. Ghosh & S. Basu, ''Nanoscale ZnO-adsorbent carefully designed for the kinetic and thermodynamic studies of Rhodamine B'', Inorganic Chemistry Communications **138** (2022) 109287. https://doi.org/10.1016/j.inoche.2022.109287.

[42] A. L. Cazetta, O. Pezoti, K. C. Bedin, T. L. Silva, A. Paesano Junior, T. Asefa & V. C. Almeida, ''Magnetic activated carbon derived from biomass waste by concurrent synthesis: Efficient adsorbent for toxic dyes'', ACS Sustainable Chemistry & Engineering **4** (2016) 1058. https://doi.org/10.1021/acssuschemeng.5b01141.

[43] L. Cong, L. Feng, X. Wei, J. Jin & K. Wu, ''Study on the adsorption characteristics of Congo red by sycamore bark activated carbon'', Environment. Technology. Resources. Proceedings of the International Scientific and Practical Conference **1** (2017) 64. https://doi.org/10.17770/etr2017vol1.2600.

[44] H. Su, X. Wang, Y. Sun, D. Xu, L. Li, C. Liu, S. Zeng & D. Sun, ''Enhancing the adsorption capacity of hematite by manganese doping: Facile synthesis and its application in the removal of Congo red'', Bulletin of the Korean Chemical Society **38** (2017) 1155. https://doi.org/10.1002/bkcs.11239.

[45] A. Somayajula, A. A. Aziz, P. Saravanan & M. Matheswaran, ''Adsorption of mercury(II) ion from aqueous solution using low-cost activated carbon prepared from mango kernel'', Asia-Pacific Journal of Chemical Engineering **8** (2013) 1. https://doi.org/10.1002/apj.1613.

[46] M. Foroughi-Dahr, H. Abolghasemi, M. Esmaili, A. Shojamoradi & H. Fatoorehchi, ''Adsorption characteristics of Congo red from aqueous solution onto tea waste'', Chemical Engineering Communications **202** (2015) 181. https://doi.org/10.1080/00986445.2013.836633.